



ELSEVIER

Available online at www.sciencedirect.com

SCIENCE @ DIRECT®

Journal of Crystal Growth 253 (2003) 38–45

JOURNAL OF
**CRYSTAL
GROWTH**

www.elsevier.com/locate/jcrysgr

Micro-X-ray fluorescence and micro-photoluminescence in InGaAsP and InGaAs layers obtained by selective area growth

A.A. Sirenko^{a,*}, C.L. Reynolds^a, L.J. Peticolas^a, A. Ougazzaden^a, A. Kazimirov^b,
Rong Huang^b, E. Fontes^b, D. Bilderback^b

^a *Agere Systems, Semiconductor Photonics Research, 9999 Hamilton Blvd., Breinigsville, PA 18031, USA*

^b *CHESS (Cornell High Energy Synchrotron Source), 277 Wilson Laboratory, Cornell University, Ithaca, NY 14853, USA*

Received 23 August 2002; accepted 13 February 2003

Communicated by R.S. Feigelson

Abstract

Properties of selective-area-grown (SAG) ternary and quaternary layers of InGaAs and InGaAsP produced by metal organic vapor phase epitaxy (MOVPE) have been investigated by using a combination of micro-photoluminescence and synchrotron-based micro-beam X-ray fluorescence techniques. Significant variations of the group-III element composition with increase of the oxide mask width and with decrease of the gap between the masks were observed in both ternary and quaternary layers. In contrast, concentration of the group-V elements in quaternary layers does not show any significant change. Effects of the SAG growth on variations of the group-III element composition become more pronounced with increase of the growth pressure.

© 2003 Elsevier Science B.V. All rights reserved.

PACS: 07.85.Q; 78.66.-w; 78.55.Cr; 81.15.Gh

Keywords: A1. Synchrotron radiation; A1. X-ray fluorescence; A3. Metalorganic vapor phase epitaxy; A3. Selective epitaxy; B1. InGaAsP-InP; B2. Semiconducting quaternary alloys

Semiconductor layers of InGaAsP and InGaAs grown selectively by metal organic vapor phase epitaxy (MOVPE) on striped regions of InP substrate surrounded by a pair of dielectric mask stripes are important building blocks for high-level integration in modern optoelectronics. By using the selective area growth (SAG) technique, differ-

ent device components with desired optical properties such as the laser and modulator sections of the electroabsorption modulator laser (EML), integrated waveguides, and laser arrays for wavelength division multiplexing (WDM) applications [1,2] can be produced in the same growth run. This level of device integration is a result of simultaneous fabrication of semiconductor materials with different thickness and composition on separate regions of the same wafer [3–5]. During MOVPE growth of InGaAsP or InGaAs layers on an oxide-patterned InP substrate, the growth reaction does not occur on the surface of the oxide mask.

*Corresponding author. Tel.: +1-484-397-3825; fax: +1-484-397-2434.

E-mail addresses: asirenko@tqs.com,
a.sirenko@hotmail.com (A.A. Sirenko),
ayk7@cornell.edu (A. Kazimirov).

Instead, precursors diffuse to the open regions of the substrate where they react and growth occurs. This in-plane diffusion process results in modification of the thickness of the semiconductor layer: there is no growth on the oxide mask and there is a significant growth enhancement in the vicinity of the oxide mask in comparison with the field region of the wafer (far from the mask). The difference in the precursor properties for the group-III elements such as diffusion coefficients D_v and surface reaction constants k for Ga and In results also in significant variation in the composition of ternary and quaternary layers in the vicinity of the oxide mask [6,7].

Details of the SAG mechanism that depend on both the geometry of the oxide mask and the growth conditions, such as temperature, choice of precursors, and reactor pressure, require more experimental and theoretical studies. Experimental information obtained with high spatial resolution on both thickness and composition variations in the grown layers is needed for modeling of the SAG process and optimization of new optoelectronic devices. Several experimental techniques have been applied lately for the analysis of SAG structures. Thickness variation was studied with transmission and scanning electron microscopy and interferometry [6], and the composition was determined by micro-photoluminescence [7,8]. Synchrotron-based X-ray micro-diffraction has been recently developed for the composition and thickness measurements [7,8] and has been applied to the SAG structures with a few microns width of the mask opening [9]. In this paper, we utilize a new experimental approach based on the combination of two non-destructive techniques, synchrotron-based micro-photoluminescence and micro-beam X-ray fluorescence, for the detailed analysis of the composition and the thickness variations in ternary and quaternary layers in a variety of SAG structures.

We investigated different quaternary $\text{In}_{1-x}\text{Ga}_x\text{As}_y\text{P}_{1-y}$ and ternary $\text{In}_{1-x}\text{Ga}_x\text{As}_y$ layers grown on 2-in InP substrates using the MOVPE technique at the growth temperature of 600°C and the growth pressures of 40 and 60 Torr. A typical SAG structure consisted of two 600 μm -long SiO_2 mask stripes with the stripe width A changed from 10 to 140 μm and the opening between two mask stripes

B varied from 15 to 80 μm . About 100 different combinations of A and B were studied. Ternary and quaternary layers had a thickness of about 0.2 μm in the field area of the wafer. The composition of the layers in the field region of the wafer was determined by high-resolution X-ray diffraction (HRXD) and conventional photoluminescence (PL). The PL spectra were measured at room temperature with a single channel spectrometer equipped with an InGaAs photodetector. The Nd:YAG laser (1.064 μm) with the pumping power density of about 200 W/cm^2 was used for PL spectra excitation. The laser spot with the size of about 4 μm allowed accurate measurements of the fundamental gap of the quaternary layer in the center of the SAG structures.

The X-ray microbeam fluorescence measurements were performed at the D1 beamline at Cornell High Energy Synchrotron Source (CHESS). The experimental setup is shown in Fig. 1. The energy of the X-ray beam from the bending magnet was tuned to 12.5 keV (above the Ga- and As-K edges) by using the double-crystal monochromator. To increase the flux, the multilayer optics with the band pass of 1.6% was used instead of the traditional Si crystal optics. The multibounce glass capillary optics designed and built at CHESS was used to produce an X-ray beam with a 1 μm spot size [10,11]. The sample was mounted on the computer-controlled ZX-stage with the surface of the sample positioned at a distance of about 100 μm from the tip of the capillary. During the measurements, the sample was scanned in 1 μm steps and the fluorescence spectrum was recorded with the energy-dispersive solid-state detector for each scan point. The integrated intensities of the Ga-K $_{\alpha}$ and As-K $_{\beta}$ were extracted from the fluorescence spectra and were normalized on the fluorescence yield measured in the field region of the wafer, i.e., where the thickness and the composition of the epitaxial layer were known based on conventional measurements of the PL gap and strain. The thickness of the epitaxial layers studied in this work was much less than the absorption lengths of the measured fluorescence lines and the incident beam that were 51, 22 and 16 μm for Ga-K $_{\alpha}$, As-K $_{\beta}$ and 12.5 keV X-rays, respectively. According to our estimation,

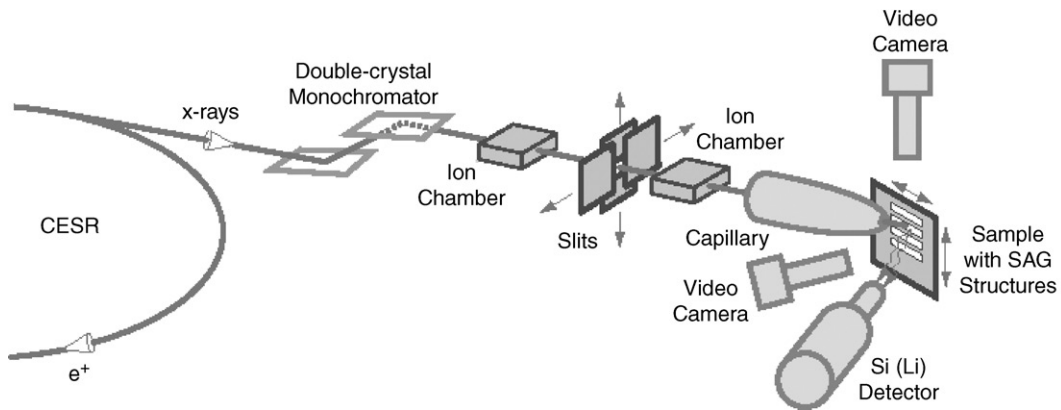


Fig. 1. Experimental setup. Synchrotron X-ray beam from the Cornell electron–positron storage ring (CESR) was monochromized by using two multilayers. The ion chambers were used to monitor the intensity of the incident beam. An X-ray beam with a $1\ \mu\text{m}$ spot size was produced by the multibounce glass capillary. The sample with SAG structures was mounted on the computer-controlled ZX-stage. Two video cameras were used to control the distance between the tip of the capillary and the sample and position of the beam on the sample. The fluorescent spectra was recorded by the Si(Li) energy-dispersive detector.

the secondary excitation of the Ga– K_α line with As– $K_{\alpha,\beta}$ photons results in a systematic increase of the Ga– K_α fluorescence by 2%, which is below the statistical error of our measurements. Moreover, this systematic error is partially corrected after normalization of the measured Ga– K_α , As– K_β fluorescence yields to the known composition of the epitaxial layer in the field region. This allows us to neglect absorption and secondary excitation effects and consider the Ga– K_α and As– K_β fluorescence yields proportional to the surface density of the fluorescing atoms. The normalized fluorescence yields of the Ga and As atoms, I_{Ga} and I_{As} , are proportional to the product of the layer thickness T and the atomic concentrations, x and y , respectively. Thus, the ratio of the corresponding intensities $I_{\text{Ga}}/I_{\text{As}}$ is independent of T and is equal to the x/y ratio. Here we assumed that the composition does not change in the growth direction for thin layers of the order of $0.2\ \mu\text{m}$ that was utilized in our experiments.

The analysis of the experimental data is different for the ternary and quaternary layers. In the case of the $\text{In}_{1-x}\text{Ga}_x\text{As}$ ternary SAG structures, the yield of the As atoms I_{As} is directly proportional to the thickness of the layer T . Then, the variation of x in the ternary layers is proportional to $I_{\text{Ga}}/I_{\text{As}}$. An example of the in-plane variation of the ternary $\text{In}_{0.47}\text{Ga}_{0.53}\text{As}$ layer composition is shown in

Fig. 1(a). The compositional map was measured with a step of $0.5\ \mu\text{m}$ in the direction perpendicular to the long edge of the oxide mask pattern and a step of $12\ \mu\text{m}$ in the direction along the oxide pads. The crosshatched regions correspond to the SiO_2 masks with a width of $10\ \mu\text{m}$. The cross section of the Ga concentration is shown in the inset of Fig. 2(a). The Ga concentration decreases gradually between the field area of the wafer and the SAG region, and the average total variation of the Ga composition is about 3%. Fig. 2(b) shows the thickness growth enhancement for the same structure. In the center of the SAG region, the thickness of the epitaxial layer is about 30% higher than that in the field region. At the edge of the mask, one can see typical thickness spikes due to formation of the triangle-like growth-enhanced areas with the sidewalls formed along (111) crystalline planes that is due to the surface migration of the group-III element precursors [4]. These thickness spikes are marked with arrows in the inset of Fig. 2(b).

To obtain the composition (x and y) of a quaternary $\text{In}_{1-x}\text{Ga}_x\text{As}_y\text{P}_{1-y}$ layer, one needs to perform at least two independent measurements. The conventional approach for analysis of macroscopic areas of quaternary layers is to measure the strain using HRXD and fundamental energy gap using PL (PL gap). Based on the system of {strain,

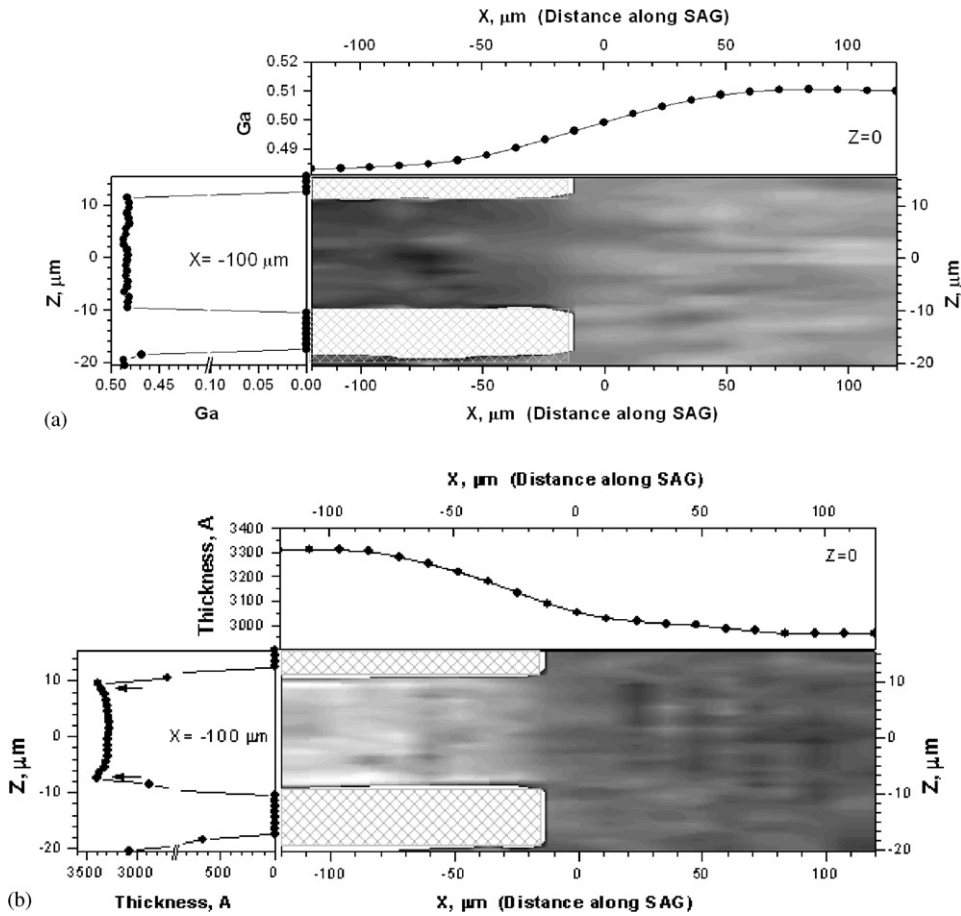


Fig. 2. In-plane variation of the Ga composition (a) and thickness (b) of the 0.26 μm -thick ternary $\text{In}_{0.47}\text{Ga}_{0.53}\text{As}$ layer grown on InP substrate by MOVPE. Both maps have been measured with a step of 0.5 μm in the direction perpendicular to the edge of the oxide mask pattern and a step of 12 μm in the direction along the oxide pads. The crosshatched regions correspond to the SiO_2 masks with the width of the mask $A = 10 \mu\text{m}$ and the distance between the masks $B = 20 \mu\text{m}$. The inserts show the cross sections of the Ga composition and thickness variation along $Z = 0$ and $X = -100 \mu\text{m}$ directions.

PL gap} values, one can obtain $\{x, y\}$ values [12,13]. In our experiments, we utilized micro-PL technique and micro-X-ray fluorescence. Using the system $\{x/y, \text{PL gap}\}$, one can obtain $\{x, y\}$ values using the same set of equations as for the $\{\text{strain}, \text{PL gap}\} \leftrightarrow \{x, y\}$ conversion. Based on that conversion, the growth rate enhancement t defined as the ratio of the thickness of the selectively grown layer and the layer thickness in the field (unperturbed) region of the wafer, can be also determined as $t = I_{\text{Ga}}/x \equiv I_{\text{As}}/y$. Thus, the combination of micro-X-ray fluorescence and micro-PL can provide a nondestructive analysis of the quaternary

layer composition and the thickness variation in SAG structures.

Figs. 3(a) and (b) show the variation of the PL gap and the strain as well as x and y composition values for the $\text{In}_{0.68}\text{Ga}_{0.32}\text{As}_{0.6}\text{P}_{0.4}$ layer in the SAG structure with $A = 140 \mu\text{m}$ and $B = 15 \mu\text{m}$. The fundamental gap wavelength shown in Fig. 3(a) increases at the vicinity of the oxide mask. The maximum of the wavelength variation between the open area (1271.5 nm) and the center of the SAG region (1347 nm) is 75.5 nm. This increase of the wavelength is mostly due to the decrease of the Ga concentration shown in

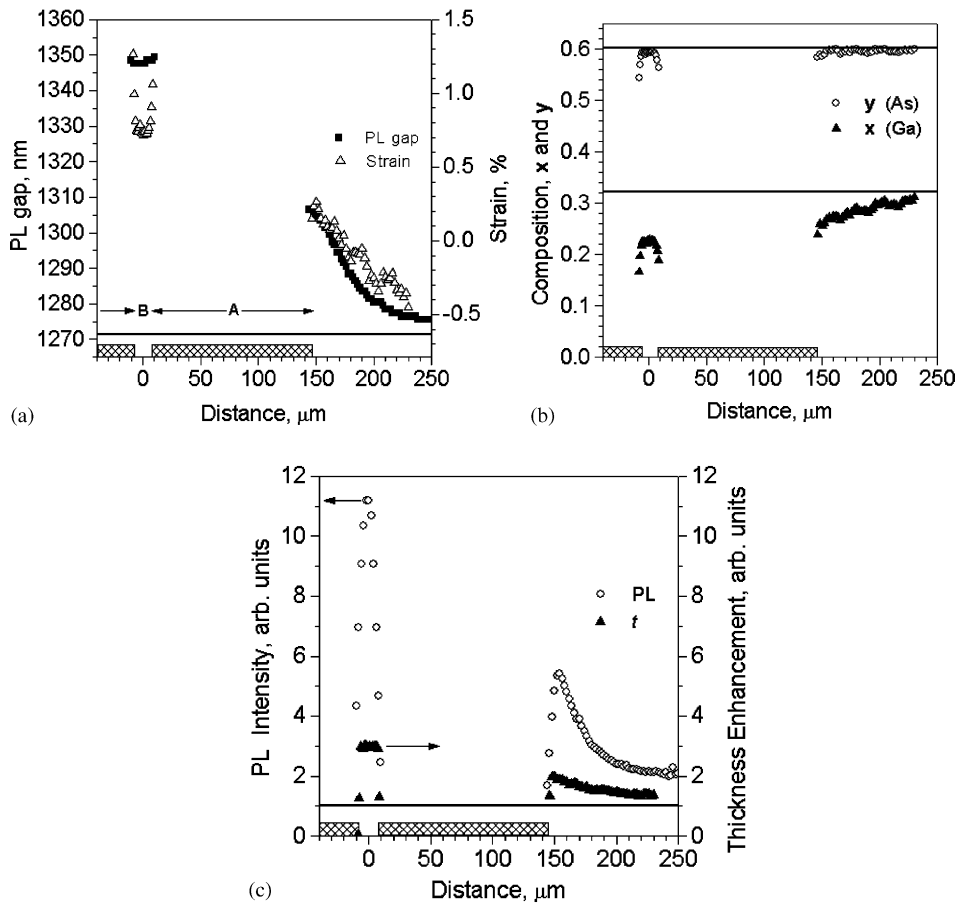


Fig. 3. (a) Variation of the optical gap (■) and strain (Δ) in the $0.14\ \mu\text{m}$ -thick $\text{In}_{0.68}\text{Ga}_{0.32}\text{As}_{0.6}\text{P}_{0.4}$ layer with the SAG structure of $A = 140\ \mu\text{m}$ and $B = 15\ \mu\text{m}$. (b) Compositions of Ga (\blacktriangle) and As (\circ) in the same SAG structure as shown in (a). (c) Variation of the PL intensity (\circ) and thickness growth enhancement (\blacktriangle) for the same SAG structure as shown in (a). The corresponding experimental values measured in the open area of the same epitaxial layer are shown schematically with the solid horizontal lines. The regions, which correspond to the SiO_2 masked area, are marked with crosshatched rectangles for clarity.

Fig. 3(b). Concentration of As in the layer is almost constant within 1% accuracy of our measurements. The drop of the As concentration within a few microns at the mask edge is an artifact both due to the spikes of the thickness enhancement (as a result of formation of the triangle-like growth-enhanced areas with the side-walls formed along (111) crystalline planes) and due to the difference in the spatial resolution of fluorescence and photoluminescence measurements. Fig. 3(c) shows variation of the PL intensity and thickness enhancement in the same SAG structure. In the center of the SAG region, the intensity of PL is about 11 times higher than

that in the field region of the sample. At the same time, the growth enhancement in this SAG structure is close to 3. To explain the difference, one should take into account that in the SAG region the strain determined by the compositional variation is positive. As a result, the PL spectrum is dominated by the heavy-hole optical transition. In contrast, the field area of this sample is negatively strained and the PL spectrum is formed by the light-hole-related optical transition. Since the interband matrix element for the heavy-hole transition is 3 times higher than that for the light hole and taking into account the experimentally determined threefold thickness enhancement, we

can explain the observed one order in magnitude increase of the PL intensity in the SAG structure. Such a high PL intensity is evidence of good crystalline quality (no relaxation) of the SAG structure with the most aggressive thickness

enhancement among the SAG structures measured in this work.

The summary of the experimental results from all mask patterns is presented in Fig. 4, which shows the composition variation and the layer

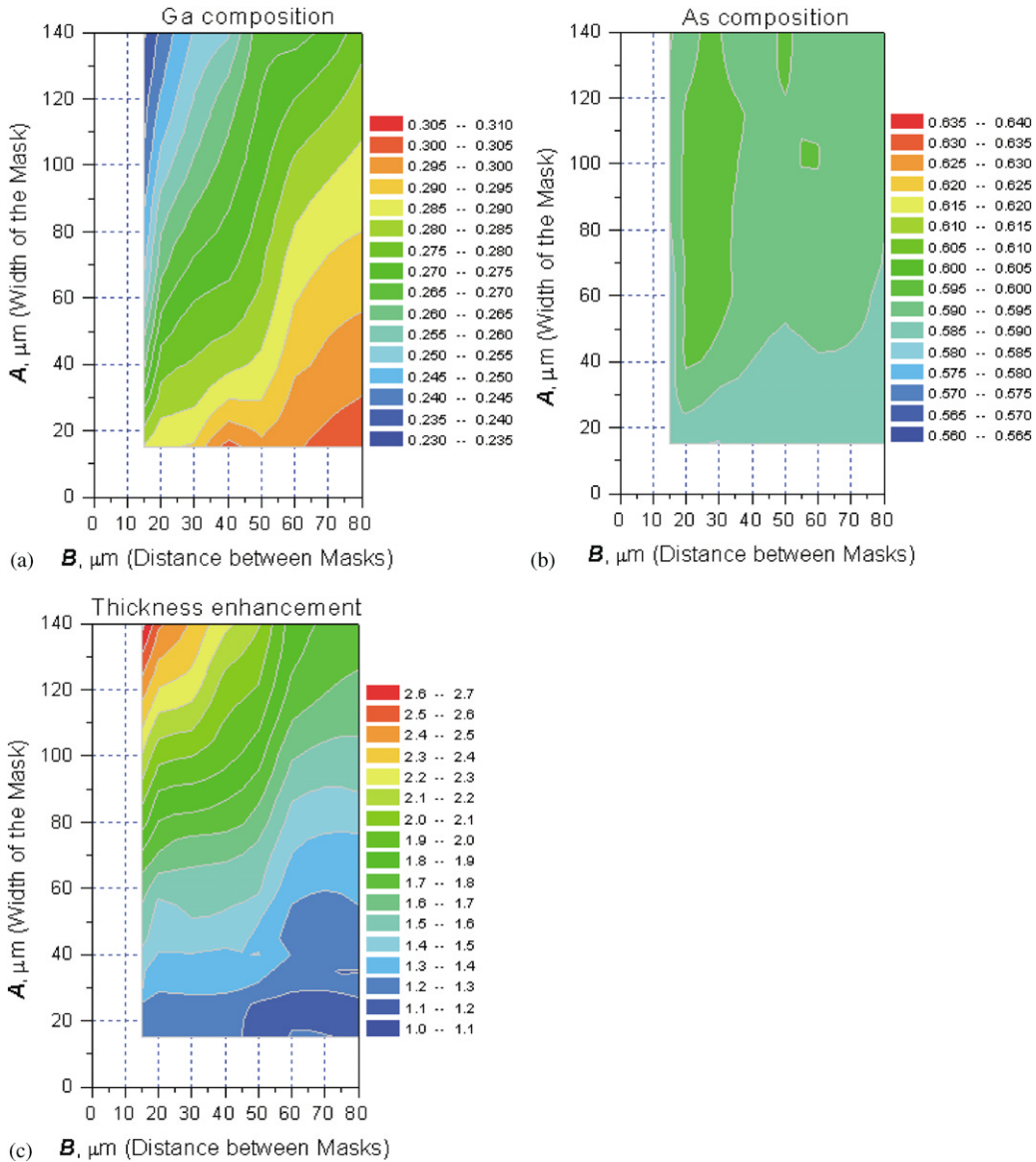


Fig. 4. Variation of the Ga and As compositions and the layer thickness enhancement (a, b, and c, respectively) measured in the centers of the SAG regions of the $0.14\mu\text{m}$ -thick $\text{In}_{0.68}\text{Ga}_{0.32}\text{As}_{0.6}\text{P}_{0.4}$ layer with different oxide mask parameters. The horizontal axis corresponds to the distance between the oxide masks B varied between 15 and $80\mu\text{m}$. The vertical axis is the width of the oxide mask A varied from 15 to $140\mu\text{m}$. The color scales for the composition variation in (a) and (b) have the same range of 0.08.

thickness enhancement in the centers of the SAG regions for a quaternary layer. The horizontal axis is the distance between the oxide stripes B and the vertical axis is the width of the oxide mask A . The upper-left corner in Fig. 4 corresponds to the most aggressive SAG condition with $B = 15 \mu\text{m}$ and $A = 140 \mu\text{m}$, while the lower-right corner approaches the properties of the field region of the sample. The direction from the upper-left to the lower-right corner in Fig. 4(a) determines the gradient of the Ga concentration. The total variation of the Ga composition is 8%. Fig. 4(b) shows As composition for the same set of the SAG structures that is measured to be constant within the accuracy of our measurements (1%). Thus we observe that the composition of the group-V elements is independent of the geometry of the SAG oxide mask and that As and P are distributed uniformly across the epitaxial layer. Even for the most aggressive SAG condition (with $B = 15 \mu\text{m}$ and $A = 140 \mu\text{m}$), the composition of As is the same as in the field region of the epitaxial layer. This result is in perfect agreement with the usual theoretical prediction based on the assumption

that D_v/k for the group-V elements is infinitely large [6]. Fig. 4(c) shows the thickness enhancement ratio. As expected, there is a clear correlation between thickness enhancement and the variation of Ga concentration, i.e. the highest thickness enhancement corresponds to the increase of In with respect to Ga composition. We fit the experimental values for the composition and thickness variation with a single set of D_v/k for the group-III elements assuming a constant composition of the group-V elements for all SAG structure dimensions. For the sample grown at 60 Torr, the best fit was obtained with $D_v/k(\text{In}) = 46 \mu\text{m}$ and $D_v/k(\text{Ga}) = 117 \mu\text{m}$ that turn out to be close to the previously reported values [7]. One should mention that, in the fitting procedure, the experimental values for the most aggressive structures have a higher weight. For example, in the structures with wide gaps ($B > 50 \mu\text{m}$) fitted alone, $D_v/k(\text{In})$ is about 50% smaller, while the best-fit values for $D_v/k(\text{Ga})$ remain unchanged.

Both the thickness and the composition of the SAG layers depend on the diffusion lengths of

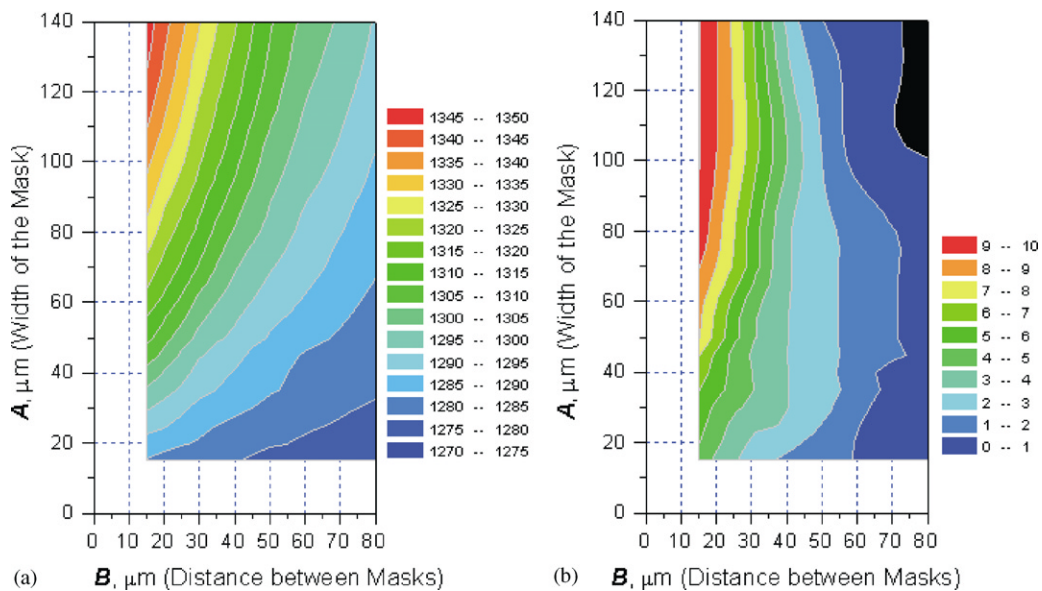


Fig. 5. (a) Variation of the PL gap of the InGaAsP SAG structures grown at 60 Torr measured in the centers of the SAG regions. The horizontal axis corresponds to the distance between the oxide masks B varied between 15 and 80 μm . The vertical axis is the width of the oxide mask A varied from 15 to 140 μm . The color scale for the PL gap variation is from 1270 to 1350 nm. (b) Difference between the PL gap variation of two samples grown at 60 and 40 Torr: PL gap(60 Torr)–PL gap(40 Torr). The color scale for the PL gap difference is from 0 to 10 nm.

reacting atoms in the gas phase that can be, at least partially, controlled by changing pressure in the MOVPE reactor. To demonstrate the effect of the growth pressure on the SAG structures, two InGaAsP layers of practically the same composition (PL gaps were the same) were grown at 40 and 60 Torr. Both samples reveal the similar behavior, i.e. the PL gap increases with both the decrease of the distance between the oxide masks and with the increase of the oxide mask width. Fig. 5(a) shows the variation of the PL gap of the SAG structure layers grown at 60 Torr. The difference between PL gap values for two samples grown at 60 and 40 Torr, $\text{PL gap}(60 \text{ Torr}) - \text{PL gap}(40 \text{ Torr})$, is plotted in Fig. 5(b). The observed difference between the variations of PL gap in these two samples means that the sample grown at lower pressure (40 Torr) has a smaller variation of the composition in the aggressive SAG structures ($B < 50 \mu\text{m}$). On the other hand, with increase in the distance between the oxide masks, the effect of the growth pressure vanishes and it is not visible for B more than $50 \mu\text{m}$. It is interesting to mention that this distance is close to the calculated D_v/k of indium.

In conclusion, a new experimental approach based on the combination of the micro-beam X-ray fluorescence and micro-photoluminescence techniques was used to study the thickness and the composition of the SAG layers grown on InP substrates at different growth conditions for a variety of oxide mask patterns. For both ternary and quaternary layers, significant variation of the group-III element composition was observed. The compositional and thickness variations increase with the increase of the mask width and the decrease of the opening between the masks. The variation of Ga concentration in the quaternary layers of 8% was measured over the entire set of the oxide patterns. Threefold thickness enhancement was observed for the most aggressive structures. In contrast, no compositional changes were recorded with respect to the group-V elements due to the large values of D_v/k for P and As. The effect of the growth pressure in the

reactor was also studied. We believe that the experimental approach developed in this paper has a great potential application for future analysis of micron-size SAG structures.

The authors gratefully acknowledge M. Hybertsen, K.E. Lutterodt, S. Ustin, and R. Leibenguth for help and useful discussions. This work is based upon research conducted at the Cornell High Energy Synchrotron Source (CHESS), which is supported by the National Science Foundation and the National Institutes of Health/National Institute of General Medical Sciences under award DMR 9713424.

References

- [1] B. Mason, A. Ougazzaden, C.W. Lentz, K.G. Glogovsky, et al., *IEEE Photon. Technol. Lett.* 14 (2002) 27.
- [2] S. Sudo, K. Kudo, K. Mori, T. Sasaki, Selective MOVPE of microarray waveguide for densely integrated photonic devices, *Conference Proceedings of the International Conference on InP and Related Materials, IPRM' 2001*, p. 390.
- [3] T. Fujii, M. Ekawa, *J. Appl. Phys.* 78 (1995) 5373.
- [4] T. Van Caenegem, I. Moerman, P. Demeester, *Prog. Crystal Growth Charact.* 35 (1997) 263.
- [5] J.E. Greenspan, X. Zhang, N. Puetz, B. Emmerstorfer, *J. Vac. Sci. Technol. A* 18 (2) (2000) 648.
- [6] M. Gibbon, J.P. Stagg, C.G. Cureton, E.J. Thrush, et al., *Semicond. Sci. Technol.* 8 (1993) 998.
- [7] M.A. Alam, R. People, E. Isaacs, C.Y. Kim, et al., *Appl. Phys. Lett.* 74 (1999) 2617.
- [8] Z.-H. Cai, W. Rodrigues, P. Ilinski, D. Legnini, B. Lai, et al., *Appl. Phys. Lett.* 75 (1999) 100.
- [9] S. Kimura, H. Kimura, K. Kobayashi, T. Oohira, K. Izumi, *Appl. Phys. Lett.* 77 (2000) 1286.
- [10] D.H. Bilderback, S.A. Hoffman, D.J. Thiel, *Science* 263 (1994) 201.
- [11] D.H. Bilderback, E. Fontes, Glass capillary optics for making X-ray beams of 0.1 to 50 microns diameter, in: E. Fontes (Ed.), *Synchrotron Radiation Instrumentation: Tenth US National Conference, AIP Conference Proceedings*, Vol. 417, 1997, pp. 147–155.
- [12] S. Adachi, *Physical Properties of III–V Semiconductor Compounds*, Wiley, New York, 1992.
- [13] I. Vurgaftman, J.R. Meyer, L.R. Ram-Mohan, *J. Appl. Phys.* 89 (2001) 5815.